ELSEVIER

Journal of Nuclear Materials 318 (2003) 241–248

journal of nuclear materials

www.elsevier.com/locate/jnucmat

Effect of implanted helium on tensile properties and hardness of 9% Cr martensitic stainless steels

P. Jung [a,*], J. Henry [b], J. Chen [a], J.-C. Brachet [b]

[a] *Institut für Festkörperforschung, Forschungszentrum Jülich, GmbH, D-52425 Jülich, Germany*
[b] *CEA/DEN/SAC/DMN/SRMA, CEA Saclay, F-91191 Gif-sur-Yvette cedex, France*

Abstract

Hundred micrometer thick specimens of 9% Cr martensitic steels EM10 and T91 were homogeneously implanted with He^4 to concentrations up to 0.5 at.% at temperatures from 150 to 550 °C. The specimens were tensile tested at room temperature and at the respective implantation temperatures. Subsequently the fracture surfaces were analysed by scanning electron microscopy and some of the specimens were examined in an instrumented hardness tester. The implanted helium caused hardening and embrittlement which both increased with increasing helium content and with decreasing implantation temperature. Fracture surfaces showed intergranular brittle appearance with virtually no necking at the highest implantation doses, when implanted below 250 °C. The present tensile results can be scaled to tensile data after irradiation in spallation sources on the basis of helium content but not on displacement damage. An interpretation of this finding by microstructural examination is given in a companion paper [J. Nucl. Mater., these Proceedings].

1. Introduction

The high energy protons and neutrons in spallation devices produce, in addition to displacement damage and other transmutation products, the light elements hydrogen and helium at concentrations, which are higher than expected in future fusion reactors by more than one order of magnitude. Helium is of especial great concern as, unlike hydrogen, it is easily immobilised and will be retained in large quantities in the structural materials. Previous investigations of the effect of helium on mechanical properties concentrated on elevated temperatures and moderate helium concentrations, representative of fission and fusion environments. The present investigations cover a wide range of temperatures (from close to room temperature to 550 °C) and extend to rather high concentrations (up to 0.5 at.%). These conditions are typical for the beam window and target area in a high power spallation source such as the planned European Spallation Source (ESS) for neutron research and the Accelerator Driven Systems (ADS) for waste transmutation. The maximum concentration (0.5 at.%) corresponds to about one-half year full power operation of these devices. In the present study helium is implanted with relatively little simultaneous production of displacement damage. This allows separation of the specific effect of helium on mechanical properties and microstructure. On the other hand this kind of simulation differs from the situation in a real device for example with respect to implantation rate and specimen thickness, with consequences for defect kinetics and fracture mechanics. For example, the He/dpa ratio in these implantation experiments exceeds those in ESS or ADS by more than one order of magnitude. On the other hand, He/dpa ratios in other simulation environments, such as fusion and fast-fission, are by more than one and three orders of magnitude lower, respectively, than in ESS/ADS [1]. The range of the implanted α-particles, corresponding to a maximum energy of 28 MeV at the Jülich cyclotron, limits the specimen thickness for steels to about 100 μm. Thicker specimens (up

* Corresponding author. Tel.: +49-2461 614036; fax: +49-2461 612410.
E-mail address: p.jung@fz-juelich.de (P. Jung).

0022-3115/03/$ - see front matter © 2003 Elsevier Science B.V. All rights reserved.
doi:10.1016/S0022-3115(03)00014-X

to about 240 μm) can be homogeneously implanted by He^3 (maximum energy 36 MeV).

The materials investigated were two martensitic 9% Cr steels which are superior to austenitics in strength and radiation resistance at elevated temperatures (swelling, irradiation creep and helium embrittlement) and for these reasons were selected as candidate materials in ESS and ADS. Measurements comprised tensile tests at room temperature and at implantation temperature, microhardness tests at room temperature and analysis of fracture surfaces by scanning electron microscopy (SEM). Disks from the tensile specimens and additionally implanted larger specimens were used for microstructural examination by transmission electron microscopy (TEM), by small angle neutron scattering (SANS) and tomography atom probe (TAP), respectively. Some of these results are described in a companion paper [2].

2. Experimental details

2.1. Materials and helium implantation

Compositions of the two steels were 8.8% Cr, 1.0% Mo, 0.2% Ni, 0.1% C (EM10) and 8.2% Cr, 1.0% Mo, 0.2% V, 0.1% Ni, 0.1% C, 0.075% Nb (T91) with average prior austenite grain sizes of 20 and 14 μm, respectively. More details on material and preparation and geometry of the 100 μm thick specimen are given in Ref. [2]. For implantation four tensile specimens were mounted on one holder at mutual separations of 1 mm for each run. The specimens were fixed on one end, while the other end was free, to avoid stresses from thermal expansion. The specimens were heated by the beam current while cooling was supplied by flowing helium gas which passed the specimens tangentially from both sides at velocities up to 100 m/s. The gas entered the apparatus through 10 adjustable nozzles and was continuously cleaned in a cooling circuit [3,4]. Temperature was adjusted by the flow rate of the gas. One specimen was electrically insulated to allow determination of average temperature along the gauge length by measurement of electrical resistivity with a current of 0.1 A. Heating by this current was negligible. Relative temperature measurement was performed by a movable infrared pyrometer directed towards the backside of the specimens at an angle of 45° with a measuring spot of about 1 mm in diameter. To obtain conditions as similar as possible for all specimens, the inner and outer tensile specimens were exchanged after accumulation of half the total dose. The holders were mounted in an irradiation apparatus at a beam line of the Jülich Compact Cyclotron. The α-beam of energy 27.4 MeV (as measured by an inductive method) passed through a 13×13 mm aperture and a 28 μm Hastelloy window. In order to achieve uniform implantation throughout the thickness, the energy of the beam, equal to 22.8 MeV behind the window, was variably degraded by a rotating wheel made of 24 aluminium foils of different thicknesses. The calculated deviation from homogeneous implantation is less than 1% [5]. For sake of homogeneity, the beam was scanned at sawtooth frequencies of typically 300 Hz in both directions across the specimens. The beam could be stopped by a shutter, which was also used for electrical measurement of the beam current. Electrical measurement of the beam current in the apparatus was not possible due to ionisation of the cooling gas. Calibration of implanted helium concentration versus current was derived previously from helium desorption experiments [6], giving a correction factor of about 0.7 to the calculation from beam current, which is ascribed to the emission of secondary electrons from the shutter.

At 250 °C, the implantation rate was limited by the available cooling power. In this case about 1 bar pressure of the helium gas was applied, giving a typical flow velocity of 100 m/s and allowing an implantation rate of 0.015 appm/s. On the other hand, at 550 °C, the implantation rate was limited by the available beam current from the cyclotron. In this case the helium pressure was typically 0.6 bar and the implantation rate 0.020 appm/s. The implantation process results in displacement damage. For homogeneous implantation into a 100 μm steel foil, an average value of 65 displacement per He atom is derived from experimental data [7], while calculations by the TRIM-code [8,9], using a displacement energy of 40 eV, give an average of 155 displacements per implanted helium atom. In the following, we will use the latter value since it allows comparing mechanical data for steels irradiated in different radiation environments on a common basis in terms of dpa by using the standard NRT model [10]. This yields about 0.8 dpa per 5000 appm He and a displacement rate of about 2.5×10^{-6} dpa/s. Experimental parameters and results are summarised in Table 1.

2.2. Tensile testing

Implanted as well as unimplanted (without additional heat-treatment) control specimens were mounted in a tensile apparatus for miniature specimens situated in a vacuum furnace at pressures below 10^{-3} Pa. Heating in the evacuated furnace took about 20 min. Relative strain rates were around 10^{-4}/s. Strains were calculated from length change, measured at the clamping, divided by the effective gauge length of about 11 mm [1]. All specimens broke in the gauge section, except for one T91 and both EM10 specimens implanted at 250 °C to 5000 appm He, which broke in the fillets. Actually the both specimens which were tested at room temperature broke on both fillets, the second breakage probably occurring by the

Table 1
Parameters of specimen and irradiation, and results of tensile, hardness and SEM measurements

Specimen	Thickness (μm)	T_{impl} (°C)	c_{He} (appm)	Dose (dpa)	T_{test}	$\sigma_{0.2}$ (MPa)	σ_{UTS} (MPa)	ε_U (%)	ε_f (%)	d_{neck} (μm)	$HV_{0.2}$
EM10	111.0	–	–	–	25	576	744	7.0	9.5	38	3.16
EM10	107	–	–	–	250	526	651	4.9	6.2	29	3.00
EM10	102	–	–	–	550	383	409	1.3	14.0	29	2.81
EM10	102.0	250	5000	0.8	25	1281	1419	0.0	0.43	99	4.23
EM10	103.0	550	5000	0.8	25	797	885	3.65	5.5	82	3.22
EM10	106.0	550	5000	0.8	550	497	514	0.66	3.3	84	2.95
T91	104.0	–	–	–	25	598	750	6.0	8.3	35	2.94
T91	97	–	–	–	150	594	704	4.95	6.63	23	–
T91	91	–	–	–	250	558	662	3.9	4.9	24	–
T91	98	–	–	–	325	547	659	5.1	5.8	28	–
T91	91	–	–	–	400	559	651	4.0	5.2	28	–
T91	106.0	–	–	–	550	368	398	1.1	16.9	27	2.79
T91	100	150	1250	0.2	25	1055	1103	0.93	1.8	36	–
T91	99	150	1250	0.2	150	1011	1028	0.39	1.47	36	–
T91	100	250	625	0.1	25	918	957	2.9	4.2	35	–
T91	100	250	625	0.1	250	783	811	2.0	2.8	41	–
T91	98.0	250	2400	0.38	25	1191	1191	0.09	1.0	48	–
T91	97	250	2400	0.38	250	901	901	0.2	0.25	37	–
T91	114.0	250	5000	0.8	25	1079	1079	0.0	0.04	111	5.05
T91	114.5	250	5000	0.8	250	1217	1248	0.33	0.62	87	5.96
T91	99	325	1250	0.2	25	860	939	2.60	4.0	40	–
T91	97	400	2500	0.4	25	858	930	2.35	4.25	37	–
T91	105	400	2500	0.4	400	632	702	2.0	3.3	44	–
T91	112.0	550	5000	0.8	25	766	867	4.4	6.3	64	3.20
T91	112.	550	5000	0.8	550	520	543	1.05	2.5	96	3.24

shock when after fracture the recoiling specimen holder hit the frame.

2.3. Scanning electron microscopy

Surface analysis by SEM was performed in a Hitachi-F800, using secondary electrons mostly from 20 kV irradiation. The quality of images from the present steels was sometimes inferior to those typical of austenitics, probably due to the magnetic specimens.

2.4. Hardness testing

Hardness testing was performed in an instrumented hardness tester [6,11] at room temperature after tensile testing. Tests were made in the gauge section, but far away from the fracture region. Force was recorded against indentation depth during measurement, allowing measurement of hardness versus indentation depth as well as Young's modulus during unloading. Microhardness values were constant above ≈0.5 N, but were slightly increasing at loads below 0.2 N. For loads above 0.5 N, no significant change was observed when a surface layer of typical 3 μm thickness was removed by polishing. This polishing gave better reproducibility of data and indentation images of better quality (within the limits mentioned above), and for these reasons, was used throughout. Most measurements were performed at loads of 2 N and averages of at least five hardness values were taken.

3. Results

3.1. Tensile properties

Fig. 1 shows tensile curves (engineering stress and strain) of T91 specimens tested at 250 °C after implantation at 250 °C to various helium concentrations c_{He}. Increases in strength and associated losses in ductility are found for increasing c_{He}. The effect of temperature is shown in Fig. 2 for T91 implanted to about 0.25 at.% He at 250 and 400 °C, respectively, and tested at the implantation temperatures. While implantation and testing at 400 °C causes only minor strengthening and loss of ductility, the 250 °C data show a large effect of implantation.

Yield strengths, ultimate tensile strengths, and elongations to fracture of 100 μm T91 specimens as a function of helium content after implantation at various temperatures are compiled in Figs. 3–5, respectively. Due to the very weak work hardening, uniform elongation is not very well defined for these materials. In Table 1 the elongation ε_{UTS} at maximum engineering

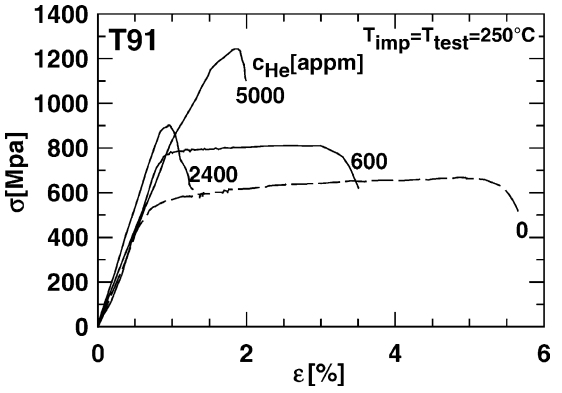

Fig. 1. Tensile curves (engineering stress and strain) of T91 specimens at 250 °C and strain rates of 8.5×10^{-5}/s, after implantation at 250 °C to helium concentrations c_{He} up to 0.5 at.%, corresponding to 0.8 dpa.

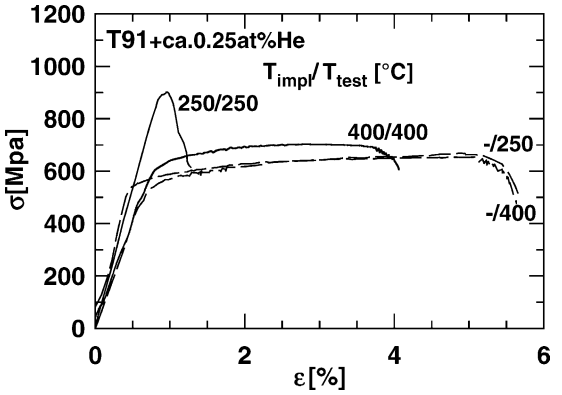

Fig. 2. Engineering tensile curves of T91 specimens with about 0.25 at.% He (0.4 dpa) after implantation and testing at 250 and 400 °C, respectively, with strain rates of 8.5×10^{-5}/s. Results of unimplanted controls are shown for comparison.

stress is given. Open and filled symbols indicate testing at room temperature and implantation temperature, respectively. For 150 and 250 °C, the strength values increase strongly for concentrations at least up to about 2500 appm, while for higher temperatures only moderate hardening is observed. At the highest concentrations, the measured maximum stresses may even be below σ_{UTS} as the specimens ruptured in the elastic region. The strain to rupture drops at the lower temperatures to below 1% above 2500 appm, while at higher temperatures it seems to level off at some finite values. Plastic energies which are estimated from $(\sigma_{0.2} + \sigma_{UTS})^* \varepsilon_{UTS}/2$, with ε_{UTS} the strain at σ_{UTS}, are given in Fig. 6.

True tensile curves of T91 and EM10 tested at 25 °C after implantation of 5000 appm He at 250 and 550 °C, respectively, are compared in Fig. 7. Similarly to Fig. 2, the effects of implantation are much more pronounced at 250 °C than at 550 °C. For 550 °C, the EM10 speci-

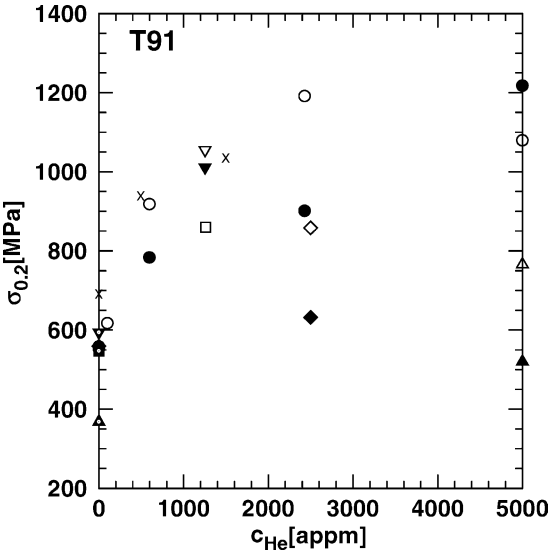

Fig. 3. Yield strengths of 100 μm T91 specimens as a function of helium content after implantation at temperatures of about 150 °C (▽), 250 °C (○), 325 °C (□), 400 °C (◇) and 550 °C (Δ). Open and filled symbols indicate testing at room temperature and implantation temperature, respectively. Crosses indicate results for Mod9Cr1Mo steel, irradiated (LANSCE) and tested at 164 °C [13].

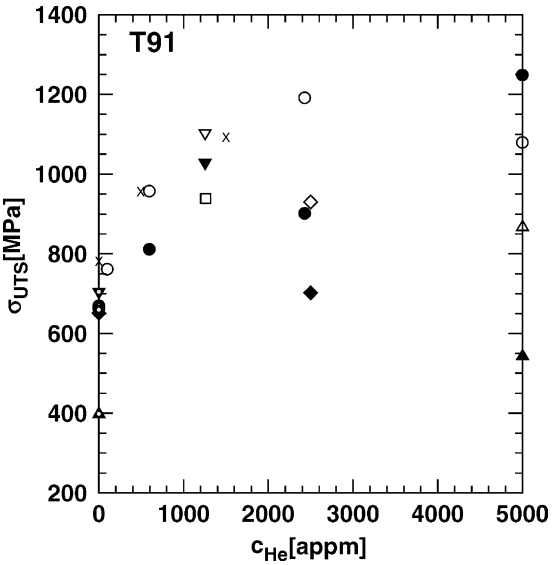

Fig. 4. Ultimate tensile strengths of 100 μm T91 specimens as a function of helium content after implantation at temperatures of about 150 °C (▽), 250 °C (○), 325 °C (□), 400 °C (◇) and 550 °C (Δ). Open and filled symbols indicate testing at room temperature and implantation temperature, respectively. Crosses indicate results for Mod9Cr1Mo steel, irradiated (LANSCE) and tested at 164 °C [13].

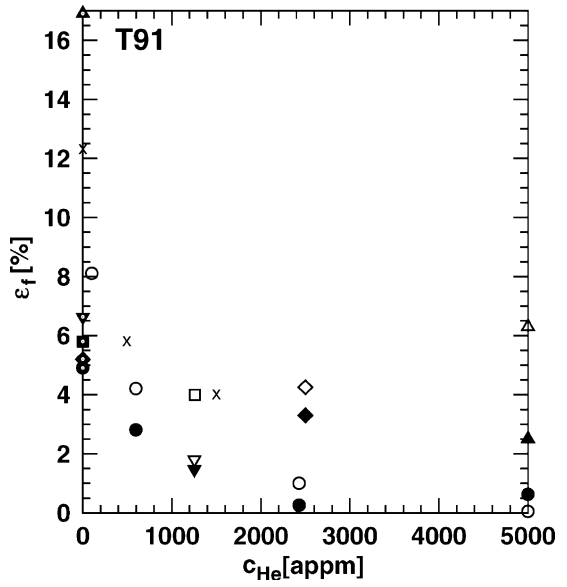

Fig. 5. Elongations to fracture of 100 μm T91 specimens as a function of helium content after implantation at temperatures of about 150 °C (▽), 250 °C (○), 325 °C (□), 400 °C (◇) and 550 °C (Δ). Open and filled symbols indicate testing at room temperature and implantation temperature, respectively. Crosses indicate results for Mod9Cr1Mo steel, irradiated (LANSCE) and tested at 164 °C [13].

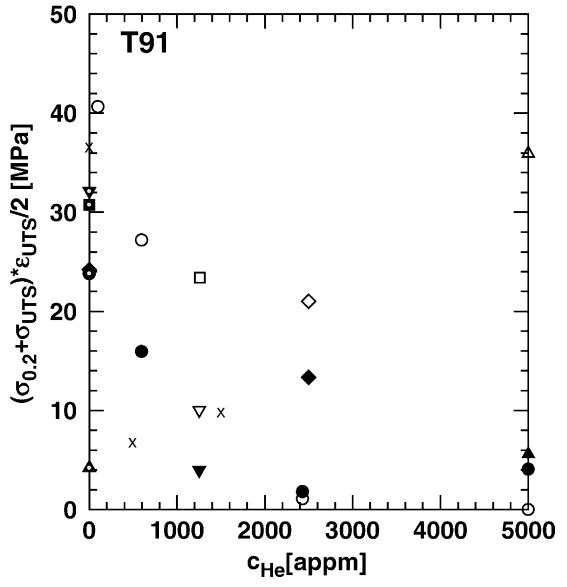

Fig. 6. Plastic energies of 100 μm T91 specimens as a function of helium content after implantation at temperatures of about 150 °C (▽), 250 °C (○), 325 °C (□), 400 °C (◇) and 550 °C (Δ). Open and filled symbols indicate testing at room temperature and at implantation temperature, respectively. Crosses indicate results for Mod9Cr1Mo steel, irradiated (LANSCE) and tested at 164 °C [13].

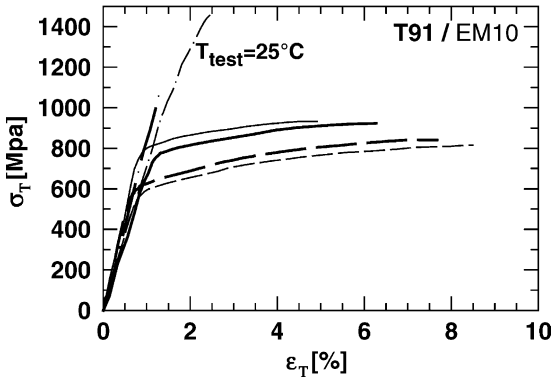

Fig. 7. Comparison of true tensile curves at 25 °C and strain rates of 8.5×10^{-5}/s for T91 (bold lines) and EM10 after implantation of 0.5 at.% He (0.8 dpa) at 250 °C (dash-dotted) and 550 °C (solid), respectively. Unimplanted controls (dashed) are given for comparison.

mens show somewhat more hardening as well as embrittlement than T91, while at 250 °C no clear comparison is possible as virtually no ductility is retained.

3.2. Fracture surfaces

The fracture surfaces of T91 (left) and EM10 (right) after implantation at 250 °C to 5000 appm He and testing at 25 °C are compared in Fig. 8. Most grains show completely intergranular fracture along the prior austenite grain boundaries. Fig. 9 shows fracture surfaces of T91 after implantation at 250 °C (a,c) and 550 °C (b, d) and testing at 25 °C (a, b) and implantation temperature (c, d), respectively. While implantation at 250 °C induces fracture without necking, some necking and ductile appearance is retained after implantation at 550 °C. For foil specimens, reduction in area can be estimated from the ratio of thickness of neck, d_{neck}, and thickness d of the specimen outside the neck by: $1 - d_{neck}/d$. Data from testing at 25 °C (open) and at the implantation temperature (filled) are given in Fig. 10, respectively.

3.3. Hardness

SEM pictures of indentations from hardness tests are shown in Fig. 11. In some cases, indications of cracking or flaking under indentation were observed (right), but in some cases this also occurred in unimplanted controls and therefore could not be clearly assigned to implantation. Load versus depth curves are shown in Fig. 12. In agreement with Figs. 1 and 7 the specimen implanted at 250 °C experienced strong hardening, while after implantation at 550 °C only a minor increase is observed. Hardness data at 2 N are compared to yield stress and of the respective specimens in Fig. 13. The

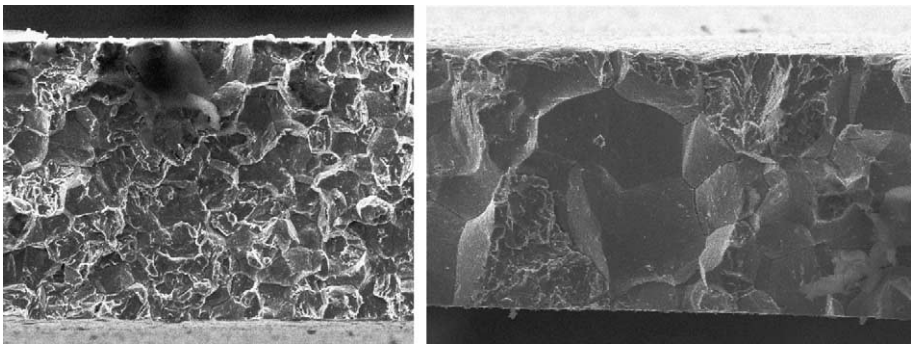

Fig. 8. Fracture surfaces of ≈100 μm T91 (left) and EM10 (right) after implantation at 250 °C to 0.5 at.% He and testing at 25 °C. Average prior austenitic grain sizes are 14 and 20 μm, respectively.

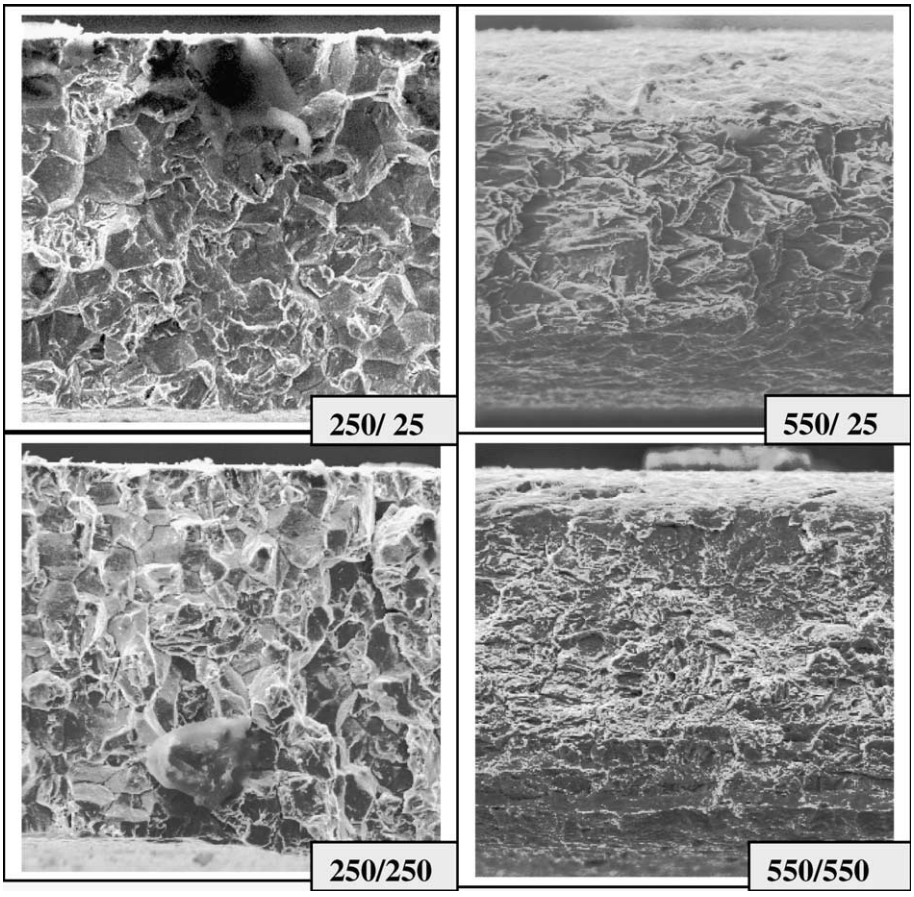

Fig. 9. Fracture surfaces of ≈100 μm T91 specimens after implantation at 250 and 550 °C and testing at 25 °C and implantation temperature (inserts), respectively.

dashed line corresponds to an empirical relation derived from a literature review in [12]. Due to the low work hardening a similar relation holds for ultimate tensile strength.

4. Discussion

It is well known that martensitic steels show much less work hardening, in comparison to austenitic stain-

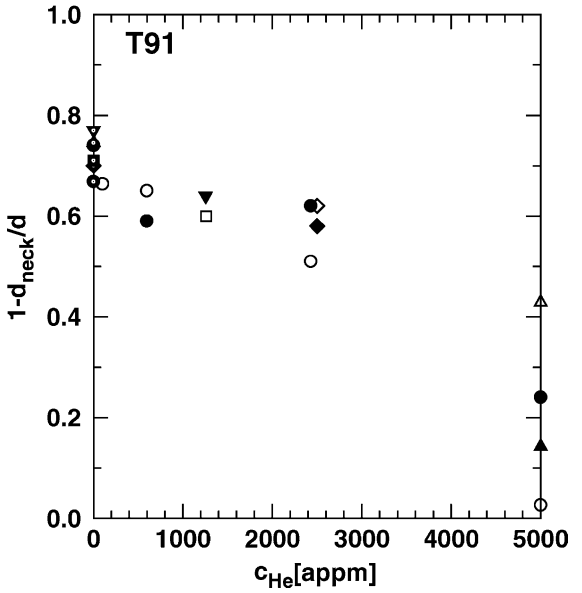

Fig. 10. Reduction of area as derived from the relative width of the neck after implantation at temperatures of about 150 °C (▽), 250 °C (○), 325 °C (□), 400 °C (◇) and 550 °C (Δ). Open and filled symbols indicate testing at room temperature and implantation temperature, respectively.

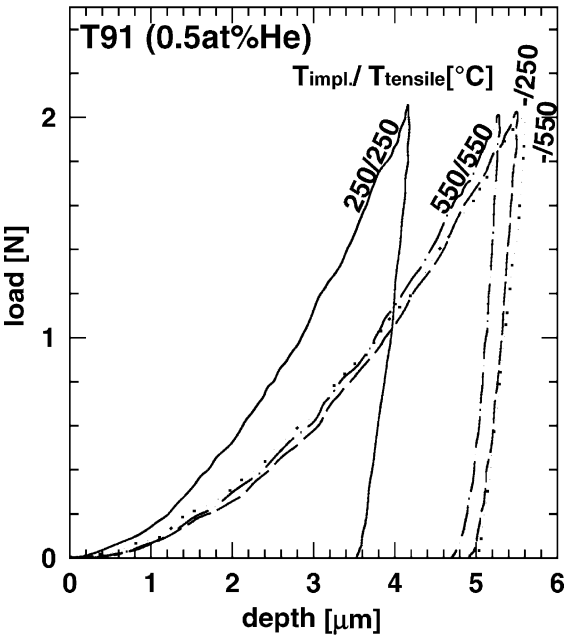

Fig. 12. Load versus depth curves during loading and unloading from instrumented hardness measurements on T91 specimens implanted and tested at 250 and 550 °C, respectively. Results from unimplanted controls are shown for comparison.

less steels. This tendency is further enhanced after irradiation, when under certain conditions work softening is observed, which may be due to localised deformation. The implanted specimens from the present study showed qualitatively similar behaviour. The present results clearly show a strong effect of implanted helium on tensile properties, mainly hardening and loss of ductility, with these effects increasing with decreasing implantation temperatures. The tensile test temperature has some but not a decisive influence on ductility. For example after implantation at 250 °C, ε_f is slightly lower in the test at room temperature compared to 250 °C, while after implantation at 550 °C the higher test temperature (550 °C) gives a somewhat higher elongation. Unfortunately, an exact comparison of the present results from helium implantation to available data from irradiation in a spallation environment is not possible, as material

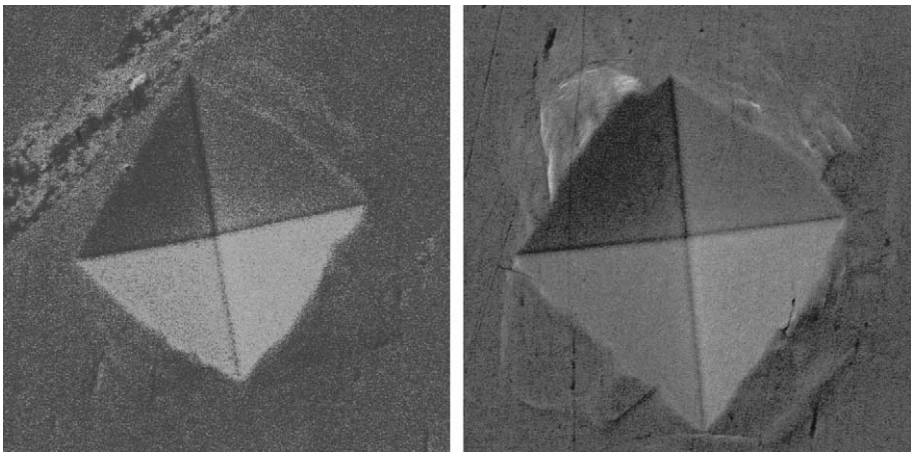

Fig. 11. SEM pictures of indentations at room temperature on EM10 after tensile testing at 25 °C, without implantation (left) and after implantation to 0.5 at.% He at 250 °C (right). The average diagonals are 42 and 38 μm, respectively.

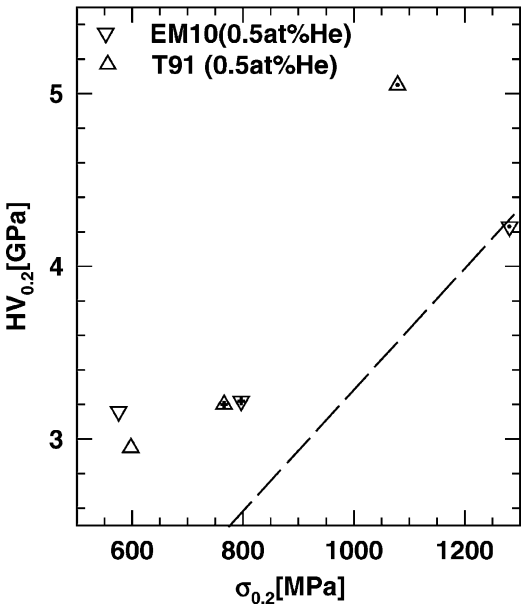

Fig. 13. Comparison of hardness at 2 N to yield strength from tensile measurements at room temperature. Empty, dotted and crossed symbols indicate unimplanted specimens and specimens implanted at 250 and 550 °C, respectively.

as well as irradiation and testing conditions are different. Data are available for mod9Cr1Mo steel, irradiated and tested at 164 °C at LANSCE [13]. In this case the displacement doses were 2.9 and 8.8 dpa, and the respective calculated helium concentrations were about 500 and 1500 appm. The corresponding tensile data are included in Figs. 3–6. The stresses (Figs. 3 and 4) from Ref. [13] are slightly above the present results for 150 and 250 °C for tests at implantation temperature (filled symbols). If differences in material and dose calculations are neglected, this may indicate some additional contribution from displacement damage to hardening, and possible from entrapped hydrogen. The elongations to fracture show the same trend as the present results, but somewhat higher absolute values, with may be ascribed to the smaller thickness of the present specimens and to the higher ductility of the 'pure' Mod9Cr1Mo. Indeed, preliminary tests after implantation on the low-activation 9% Cr martensitic steel EUROFER97 gave also higher elongations, but qualitatively similar results as the T91 steel. It is obvious that plotting of the present results (maximum dose of 0.8 dpa for 5000 appm He) and those of Ref. [13] as a function of dpa would give no agreement. Therefore, helium implanted in martensitic steels reduces elongation and induces brittle intergranular fracture at low temperatures to an extent, which is not observed without helium, even at much higher displacement doses. Detailed comparison of tensile data from irradiations in fission and spallation environments indicate significant effects of helium for austenitic stainless steels [14], but only minor effects for ferritic/martensitic steels [15].

5. Conclusions

- The results from tensile tests as well as fracture surface analysis indicate strong embrittlement of the investigated martensitic stainless steels by implanted helium.
- The differences between the two steel species (EM10, T91) reflect mainly the difference in grain size and not the compositional variation.
- Embrittlement increases with decreasing implantation temperature.
- Hardness correlates qualitatively with tensile results.
- More results on fracture, e.g. from impact tests are needed.
- It must be investigated to what extent the embrittlement by helium is influenced by the co-implantation of hydrogen, corresponding to the simultaneous production of these species by transmutation.

References

[1] P. Jung, J. Phys. IV France 12 (2002) Pr8-59.
[2] J. Henry, M.-H. Mathon, P. Jung, these Proceedings. doi:10.1016/S0022-3115(03)00118-1.
[3] P. Jung, J. Viehweg, C. Schwaiger, Nucl. Instr. and Meth. 154 (1978) 207.
[4] P. Jung, A. Schwarz, H.K. Sahu, Nucl. Instr. and Meth. A 234 (1985) 331.
[5] Z. He, P. Jung, Nucl. Instr. and Meth. B 166&167 (2000) 165.
[6] J. Chen, P. Jung, Report KFA Jülich, Jül-2822 (1993) ISSN 0944-2952.
[7] P. Jung, in: H. Ullmaier (Ed.), Atomic Defects in Metals, Landolt-Börnstein, New Series, Group III, vol. 25, Springer, Berlin, 1991, p. 1.
[8] J.P. Biersack, L.G. Haggmark, Nucl. Instr. and Meth. 174 (1980) 93.
[9] J.F. Ziegler, Manual of TRIM Version 95.4, March 1995, unpublished.
[10] M.J. Norgett, M.T. Robinson, I.M. Torrens, Nucl. Eng. Des. 33 (1975) 50.
[11] J. Chen, P. Jung, J. Nucl. Mater. 212–215 (1994) 559.
[12] P. Jung, A. Hishinuma, G.E. Lucas, H. Ullmaier, J. Nucl. Mater. 232 (1996) 186.
[13] S.A. Maloy, M.R. James, G. Willcutt, W.F. Sommer, M. Sokolov, L.L. Snead, M.L. Hamilton, F.A. Garner, J. Nucl. Mater. 296 (2001) 119.
[14] S.A. Maloy et al., these Proceedings. doi:10.1016/S0022-3115(03)00087-4.
[15] K. Farrell, T.S. Byun, these Proceedings. doi:10.1016/S0022-3115(03)00102-8.